

Commensurability oscillations in the rf conductivity of unidirectional lateral superlattices: measurement of anisotropic conductivity by coplanar waveguide

Akira Endo,* Toshiyuki Kajioaka, and Yasuhiro Iye
The Institute for Solid State Physics, The University of Tokyo,
5-1-5 Kashiwanoha, Kashiwa, Chiba 277-8581, Japan
 (Dated: August 28, 2012)

We have measured the rf magnetoconductivity of unidirectional lateral superlattices (ULSLs) by detecting the attenuation of microwave through a coplanar waveguide placed on the surface. ULSL samples with the principal axis of the modulation perpendicular (S_{\perp}) and parallel (S_{\parallel}) to the microwave electric field are examined. For low microwave power, we observe expected anisotropic behavior of the commensurability oscillations (CO), with CO in samples S_{\perp} and S_{\parallel} dominated by the diffusion and the collisional contributions, respectively. Amplitude modulation of the Shubnikov-de Haas oscillations is observed to be more prominent in sample S_{\parallel} . The difference between the two samples is washed out with the increase of the microwave power, letting the diffusion contribution govern the CO in both samples. The failure of the intended directional selectivity in the conductivity measured with high microwave power is interpreted in terms of large-angle electron-phonon scattering.

PACS numbers: 73.43.Qt, 73.23.-b, 73.50.Mx

I. INTRODUCTION

Radio-frequency (rf) conductivity has proven to be an incisive probe to investigate a two-dimensional electron gas (2DEG) subjected to a quantizing magnetic field,¹ comprising a unique tool to detect the pinning modes of various electron-solid-like ground states as resonant peaks seen in the frequency dependence. The states thus observed encompass Wigner crystals at small fillings of the lowest Landau level²⁻⁴ or in the close vicinity of integer^{5,6} and fractional⁷ fillings, a Skyrme crystal,⁸ and bubble⁹⁻¹¹ and stripe^{12,13} phases formed at the partial fillings of high ($N \geq 2$) Landau levels. In these studies, rf conductivity is evaluated by measuring the power transmission \mathcal{T} through a coplanar waveguide (CPW)¹⁴ placed on the surface of the 2DEG wafer (see Fig. 1(a)). Microwave attenuates by coupling with the 2DEG underneath the slots of the CPW (Fig. 1(b)). Since the absorbed power increases with increasing longitudinal conductivity $\sigma_{\alpha\alpha}$ ($\alpha = x, y$) of the 2DEG, lower \mathcal{T} signifies higher $\sigma_{\alpha\alpha}$ (see Eqs. (3), (4) below). The component $\sigma_{\alpha\alpha}$ thus measured is naively expected to represent the conduction along the direction of the microwave electric field E_{rf} , perpendicular to the propagation direction of the microwave (see Fig. 1(a)). Although the direction does not matter when the conductivity is isotropic within the 2DEG plane (x - y plane), it becomes necessary to identify the direction α correctly in the measurement of states having anisotropic conductivity, as is the case with the stripe phase at the half fillings of high Landau levels.^{12,13}

In the present study, we measure, employing the CPW method, rf magnetoconductivity of unidirectional lateral superlattices (ULSLs), the systems deliberately made anisotropic by introducing one-dimensional periodic potential modulation, $V(x) = V_0 \cos(2\pi x/a)$. (We henceforth define the direction of the principal axis of the modulation as the x direction, regardless of the propagation

direction of the microwave.) By measuring samples with known anisotropy, we can identify the component of the conductivity detected in the measurement.

It is well known that ULSLs exhibit magnetoresistance oscillations — the commensurability oscillations (CO) — originating from the commensurability between the period a of the modulation and the cyclotron radius $R_c = \hbar k_F / (eB)$ with $k_F = \sqrt{2\pi n_e}$ the Fermi wavenumber and n_e the areal electron density.¹⁵ The commensurability manifests itself via two different routes: diffusion and collisional contributions.¹⁶ Although both contributions can be traced back to the same origin, the oscillations with the magnetic field of the Landau bandwidth,

$$V_B \simeq V_0 \frac{1}{\pi} \sqrt{\frac{a}{R_c}} \cos\left(\frac{2\pi R_c}{a} - \frac{\pi}{4}\right) \quad (1)$$

they differ markedly in their anisotropy, the phase, and the amplitude. The diffusion contribution $\Delta\sigma_{yy}^{\text{dif}}$ arises from the drift velocity in the y direction $v_{d,y}$ due to the dispersion of the Landau band. Accordingly, only σ_{yy} component ($\alpha = y$) exists, and $\Delta\sigma_{yy}^{\text{dif}}$ vanishes, leading to minima in σ_{yy} , at the flat band conditions,

$$\frac{2R_c}{a} = n - \frac{1}{4} \quad (n = 1, 2, 3, \dots), \quad (2)$$

where the bandwidth Eq. (1) equals zero. The collisional contribution $\Delta\sigma_{\alpha\alpha}^{\text{col}}$, on the other hand, results from the oscillations of the density of states and is therefore isotropic (seen equally in both σ_{xx} and σ_{yy} components), and takes maxima at the flat band conditions. Thus, $\Delta\sigma_{yy}^{\text{dif}}$ and $\Delta\sigma_{\alpha\alpha}^{\text{col}}$ oscillate with the same frequency (periodic in $1/B$) but with the opposite phase. The oscillation amplitude is usually much larger for the diffusion contribution, letting $\Delta\sigma_{yy}^{\text{dif}}$ dominate the oscillations in the experimental configuration in which σ_{yy} component can be detected. By examining the phase of CO (whether minima or maxima are observed at the flat band conditions),

therefore, one can see whether or not the σ_{yy} component is involved in the measured conductivity.

We study two ULSL samples, S_{\perp} and S_{\parallel} , differing in the orientation of the modulation. From the CO observed in these samples, we will show that for low microwave power the measured conductivity reflects the direction of E_{rf} as expected. With the increase of the microwave power, however, the component of the conductivity diverted from the direction of E_{rf} becomes mixed in and the oscillations are dominated by $\Delta\sigma_{yy}^{\text{dif}}$ for both samples.

We note in passing that the great volume of CO reported thus far have been observed in the resistivity. The present study represents, to the knowledge of the present authors, the first observation of CO directly in the conductivity.

The paper is organized as follows. In Sec. II, details of the experimental setup and the method of the measurement are described. Experimentally obtained rf magnetoconductivity traces exhibiting CO and the Shubnikov-de Haas oscillations (SdHO) are presented in Sec. III, which reveal that the difference between samples S_{\perp} and S_{\parallel} fades away with the increase of the microwave power. The origin of the loss of the intended orientational selectivity in the conductivity measurements is discussed in Sec. IV, followed by concluding remarks in Sec. V.

II. EXPERIMENTAL DETAILS

The devices for the measurements were fabricated from a conventional GaAs/AlGaAs 2DEG wafer (mobility $\mu = 100 \text{ m}^2\text{V}^{-1}\text{s}^{-1}$ and the electron density $n_e = 3.8 \times 10^{15} \text{ m}^{-2}$) with the 2DEG plane residing at the depth $d = 60 \text{ nm}$ from the surface. As depicted in Fig. 1, a metallic CPW having a center electrode (width $s = 40 \text{ }\mu\text{m}$) flanked by two slots with the width $w = 28 \text{ }\mu\text{m}$ and the length $l = 1.6 \text{ mm}$, designed to have the characteristic impedance $Z_0 = 50 \text{ }\Omega$, was deposited on the surface using standard electron-beam (EB) lithography technique. Two ULSL samples, S_{\perp} and S_{\parallel} schematically illustrated in Fig. 1(c), were prepared: in S_{\perp} (S_{\parallel}), x axis, namely the principal axis of the modulation, is set perpendicular (parallel) to the direction of the microwave electric field E_{rf} ; the sample S_{\perp} (S_{\parallel}) is originally designed to be sensitive to σ_{yy} (σ_{xx}). We also prepared a device without modulation, S_0 , and confirmed that oscillatory phenomena attributed to the modulation in Sec. III were absent in this sample. In ULSL samples, modulation was introduced by placing a grating of EB-resist on the slot regions of the surface. As in our previous studies,^{17–19} the grating introduces potential modulation into the 2DEG via strain-induced piezoelectric effect.²⁰

Measurements were performed in a top-loading dilution refrigerator using a probe equipped with rigid coaxial cables. Samples were immersed in the mixing chamber held at $T_{\text{bath}} = 50 \text{ mK}$ during the measurement. Microwave transmission \mathcal{T} was measured with a network analyzer (Agilent Technology E5062) for various powers

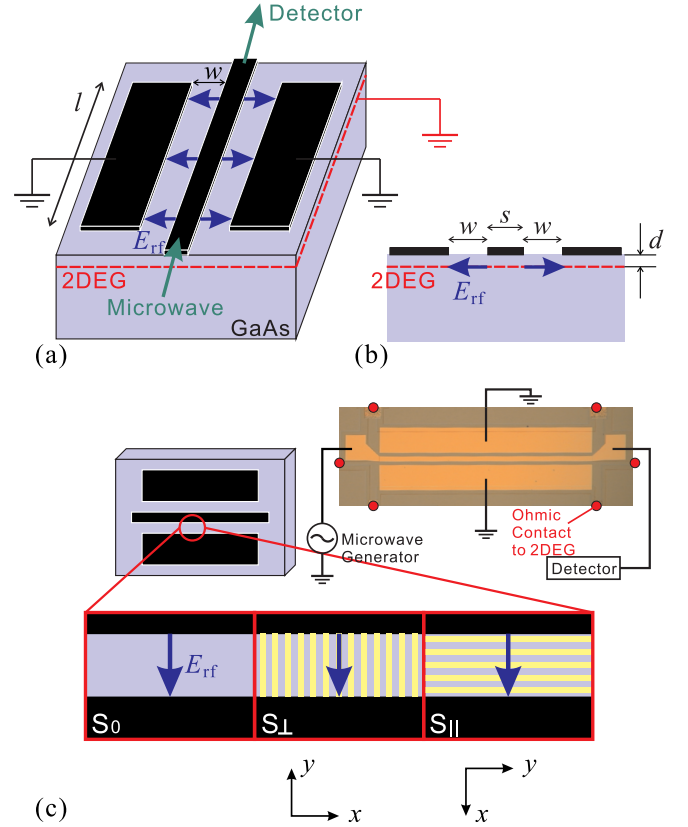


FIG. 1. (Color online) (a) Schematic drawing of the device used in the measurements. (b) Cross section of (a). Microwave transmission through a coplanar waveguide (CPW, depicted by black plates) is measured. The microwave electric field E_{rf} interacts with 2DEG beneath the two slots (width $w = 28 \text{ }\mu\text{m}$ and length $l = 1.6 \text{ mm}$) between the CPW plates. The resulting microwave attenuation reflects the conductivity of the 2DEG. (c) Illustration of the introduction of unidirectional modulation into the 2DEG in the slot region. In samples S_{\perp} and S_{\parallel} , modulation is introduced with its principal axis (x axis) perpendicular and parallel to E_{rf} , respectively. Sample S_0 is for reference (without modulation). Inset: Optical micrograph of the whole device containing six Ohmic contacts for the resistivity measurements.

P_{NA} . We used the microwave frequency $\omega/(2\pi) = 260$ or 300 MHz in the present study. No difference was observed between the two frequencies. Typical magnetic-field dependence of the transmission $\mathcal{T}(B)$ is shown in Fig. 2(a), taken for sample S_{\perp} with three different values of P_{NA} at the frequency 260 MHz . The power imparted to the electrons during the measurement inevitably heats up the 2DEG to the electron temperature T_e higher than T_{bath} ; the resultant T_e is higher for higher microwave power. For traces taken with lower powers $P_{\text{NA}} = -30$ and -45 dBm and hence having lower T_e , SdHO are clearly observed. In the close-up shown in Fig. 2(b), slower oscillations are also discernible, albeit very faintly. Oscillations are absent in the trace for the highest power $P_{\text{NA}} = 0 \text{ dBm}$, apparently having considerably high temperature $T_e \gtrsim 10 \text{ K}$. More quantitative estimate of T_e will be

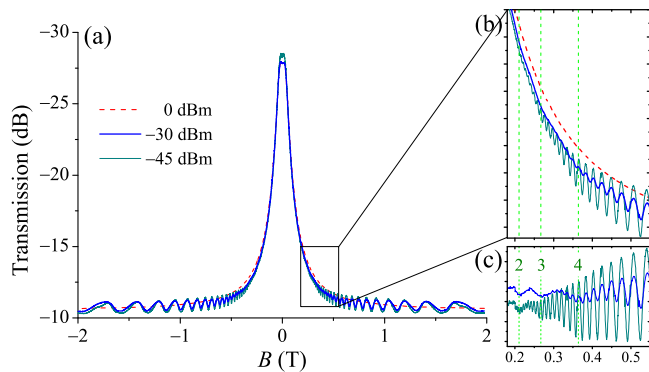


FIG. 2. (Color online) (a) Microwave transmission $\mathcal{T}(B)$ for sample S_{\perp} measured with a network analyzer, with the power (the output power of the network analyzer) $P_{\text{NA}} = -45, -30$, and 0 dBm. The transmission is plotted in such a way that the upper side represents lower power transmission (higher attenuation, corresponding to higher conductivity σ_{yy} of the 2DEG). $T_{\text{bath}} = 50$ mK. (b) Enlarged plot of the portion surrounded by the rectangle in (a). (c) Oscillatory part of the traces for -30 and -45 dBm in (b), obtained by subtracting the featureless trace for 0 dBm. The flat band conditions, Eq. (2), are indicated by vertical dashed lines in (b) and (c) along with the index n .

given below in Sec. IV. The trace for $P_{\text{NA}} = 0$ dBm can be used as the slowly-varying background for the other traces. The oscillatory part thus extracted, shown in Fig. 2(c), reveals that the slower oscillations have minima at the flat band conditions, Eq. (2), and therefore is interpreted as the CO mainly due to the diffusion contribution $\Delta\sigma_{yy}^{\text{dif}}$. The dominance of the σ_{yy} component is in accord with the expectation from the experimental setup.

The microwave with power P_{NA} generated at the network analyzer (NA) attenuates during the propagation not only along the CPW but also along the entire circuitry (coaxial cables and connectors) that connects the sample and NA, before entering the NA again to be detected. For a quantitative account of the conductivity, therefore, it is necessary to extract the contribution due to the 2DEG from the measured transmission $\mathcal{T}(B)$. This is done by noting that a 2DEG does not absorb microwave when it is not conducting, $\sigma_{\alpha\alpha} = 0$. We single out the contribution attributable to the 2DEG $\Delta\mathcal{T}(B) = \mathcal{T}(B) - \mathcal{T}(\sigma_{\alpha\alpha} = 0)$ by subtracting $\mathcal{T}(\sigma_{\alpha\alpha} = 0)$ taken from the transmission at the quantum Hall plateau, e.g., $\mathcal{T}(B)$ at $B \sim 2$ T in Fig. 2, assuming that the transmission outside the CPW does not depend on B . By using the $\Delta\mathcal{T}(B)$ thus extracted and the standard distributed-circuit theory of the microwave transmission lines,^{21,22} one obtains

$$\sigma_{\alpha\alpha} = -\frac{w}{2lZ_0} \ln \mathcal{P} \sqrt{1 + \left(\frac{v_{\text{ph}}}{2l\omega} \ln \mathcal{P}\right)^2}, \quad (3)$$

where $\mathcal{P} = P_{\text{out}}/P_{\text{in}}$ is the ratio of the microwave power leaving P_{out} and entering P_{in} the CPW, with $\ln \mathcal{P} (< 0)$

related to $\Delta\mathcal{T}$ (in dB) as

$$\ln \mathcal{P} = \ln \left(\frac{P_{\text{out}}}{P_{\text{in}}} \right) = \left(\frac{\ln 10}{10} \right) \Delta\mathcal{T}, \quad (4)$$

and $v_{\text{ph}} = 1.12 \times 10^8$ m/s represents the phase velocity. For a large enough angular frequency ω and/or a small enough $|\ln \mathcal{P}|$ (corresponding to small enough $\sigma_{\alpha\alpha}$), Eq. (3) can further be simplified as $\sigma_{\alpha\alpha} \simeq -w \ln \mathcal{P} / (2lZ_0)$, which is usually a good approximation for measurements performed at high magnetic fields deep in the quantum Hall regime, where $\sigma_{\alpha\alpha}$ is small.^{1-13,22} In the magnetic field range encompassed in the present study, however, $\sigma_{\alpha\alpha}$ remains relatively large. Furthermore, we had to resort to a relatively low frequency $\omega/(2\pi) \leq 300$ MHz in order to retain a high s/n ratio that allows us to detect the small amplitude oscillations superposed on a large background. We therefore adhere to Eq. (3) in evaluating the conductivity from $\Delta\mathcal{T}$.

III. COMMENSURABILITY OSCILLATIONS AND AMPLITUDE MODULATION OF SHUBNIKOV-DE HAAS OSCILLATIONS

In Fig. 3(a), we show the oscillatory part of the conductivity for sample S_{\perp} for lower powers $P_{\text{NA}} = -45$ and -30 dBm. The traces are obtained by first translating the transmission shown in Fig. 2(a) into the conductivity using Eqs. (3) and (4), and then by subtracting the slowly-varying background.²³ As can be seen from Eqs. (3) and (4), the dependence of the conductivity on the transmission evolves from $\propto |\Delta\mathcal{T}|$ to $\propto |\Delta\mathcal{T}|^2$ with the increase of $|\Delta\mathcal{T}|$. In other words, the sensitivity of the transmission to the conductivity decreases with increasing $|\Delta\mathcal{T}|$, or equivalently with increasing conductivity. This accounts for the larger oscillation amplitude and the higher noise level seen in the lower magnetic field regime in Fig. 3(a) compared to Fig. 2(c).

Two sets of the oscillations, SdHO and CO, are apparent in Fig. 3(a), with the former superposed on the latter. To gain more insight into those oscillations, the amplitude and the midpoint of the SdHO are drawn out as the half difference and the average, respectively, of the upper and lower envelop curves (plotted by dotted lines in Fig. 3(a)), and are shown in Fig. 3(b). The midpoint of SdHO, essentially corresponding to the CO, takes minima at the flat band conditions, consistent with the $\Delta\sigma_{yy}^{\text{dif}}$ as already mentioned in Sec. II. The amplitude of the SdHO also exhibits oscillations with the maxima occurring at the flat band conditions (most obvious at $n = 5$ and 4) for $P_{\text{NA}} = -45$ dBm. Amplitude modulation is less clear for $P_{\text{NA}} = -30$ dBm having much smaller SdH amplitude owing to higher T_e .

The modulation of the SdHO amplitude in ULSs derives from basically the same origin as CO, the diffusion and the collisional contributions.^{16,19} The diffusion contribution, namely the effect of $v_{d,y}$ on the SdHO, affects only the σ_{yy} component, and enhances the SdHO

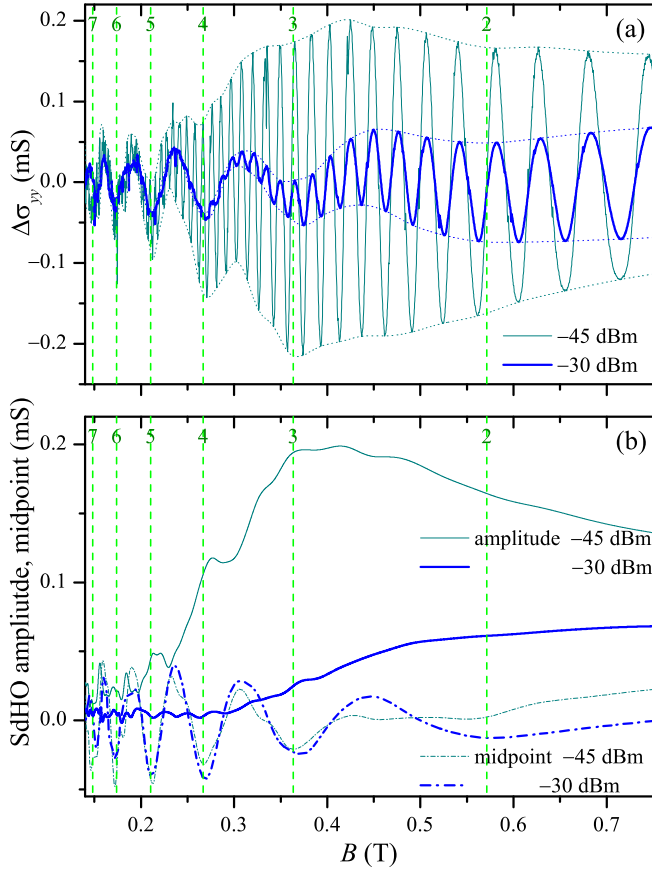


FIG. 3. (Color online) (a) Oscillatory part of the conductivity (at 260 MHz) for sample S_{\perp} (having the configuration designed to measure the σ_{yy} component) for $P_{NA} = -45$ and -30 dBm. Upper and lower envelop curves, $\Delta\sigma_{UE}$ and $\Delta\sigma_{LE}$, are shown by dotted lines. (b) Amplitude (solid lines, $(\Delta\sigma_{UE} - \Delta\sigma_{LE})/2$) and midpoint (dot-dashed lines, $(\Delta\sigma_{UE} + \Delta\sigma_{LE})/2$) of the SdHO. The flat band conditions, Eq. (2), are indicated by vertical dashed lines along with the index n .

amplitude with the increment proportional to V_B^2 , leading to the amplitude minima at the flat band conditions. The collisional contribution, by contrast, alters the SdHO amplitude isotropically. The SdHO amplitude is maximized at the flat band conditions, since there the broadening of the Landau levels (Landau bands) due to the dispersion vanishes. Again, the two contributions counteract each other. The maxima in the SdHO amplitude at the flat band conditions in Fig. 3(b) therefore signal the dominance of the collisional contribution. In a previous publication,¹⁹ the present authors have shown that the modulation of the SdHO amplitude in the magnetoresistance of ULSs is dominated by the collisional contribution at low magnetic fields and that the diffusion contribution grows rapidly with the magnetic field and becomes the dominant contribution above ~ 0.3 T. The behavior of the SdHO here is basically in line with that observed in the magnetoresistance.¹⁹ The peak of the SdHO amplitude is less apparent at $n = 3$ compared

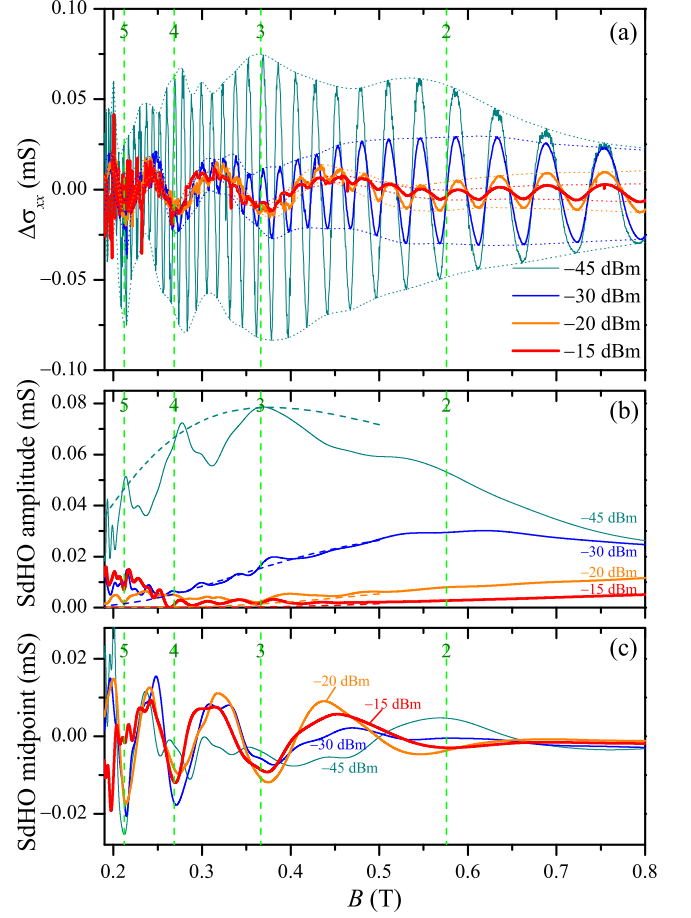


FIG. 4. (Color online) (a) Oscillatory part of the conductivity (at 300 MHz) for sample S_{\parallel} (having the configuration designed to measure the σ_{xx} component) for $P_{NA} = -45$, -30 , -20 , and -15 dBm. Upper and lower envelop curves, $\Delta\sigma_{UE}$ and $\Delta\sigma_{LE}$, are shown by dotted lines. (b) Amplitude, $(\Delta\sigma_{UE} - \Delta\sigma_{LE})/2$, of the SdHO. Dashed curves show the fitting to Eq. (6) of the values at the flat band conditions. (c) Midpoint, $(\Delta\sigma_{UE} + \Delta\sigma_{LE})/2$, of the SdHO. The flat band conditions, Eq. (2), are indicated by vertical dashed lines along with the index n .

to the peaks at $n = 5$ and 4 , which can be explained by the increase with the magnetic field of the relative importance of the diffusion contribution acting against the collisional contribution.

We now turn to sample S_{\parallel} having the modulation axis parallel to E_{rf} . First, we focus on the conductivity measured with the lowest power $P_{NA} = -45$ dBm (thinnest traces in Fig. 4). As shown in Fig. 4(a), the conductivity exhibits prominent SdHO. Amplitude modulation, with the maxima at the flat band conditions (Fig. 4(b)), is much more pronounced compared to that in sample S_{\perp} (Fig. 3(b)). The SdHO midpoint plotted in Fig. 4(c) also exhibits maxima at the flat band conditions. These observations can be consistently understood by assuming that only the σ_{xx} component is detected, as expected from the experimental configuration. The large ampli-

tude modulation of the SdHO can be ascribed to the collisional contribution in the absence of the counteracting diffusion contribution. The behavior of the SdHO midpoint (representing CO) is also attributable to the collisional contribution, which would have been wiped out if the diffusion contribution were dominant.

With the increase of the microwave power P_{NA} , however, the diffusion contribution comes into play. As can be seen in Fig. 4(c), maxima at the flat band conditions observed in the SdHO midpoint turn into minima, implying that the collisional contribution in the CO is overridden by the diffusion contribution; the σ_{yy} component dominated by the diffusion contribution $\Delta\sigma_{yy}^{\text{dif}}$ gets mingled in the conductivity measured with the setup aimed at probing σ_{xx} .²⁴ We will consider the origin of the mixing of the component deflected from the direction of E_{rf} in Sec. IV.

IV. ORIENTATIONAL SELECTIVITY IN THE CONDUCTIVITY MEASUREMENT

In this section, we examine the role played by electron-phonon scattering in the process of electron heating by the microwave absorption. Since the electron-phonon scattering is a major source of large-angle scattering in 2DEGs, it is expected to significantly affect the directivity of the conductivity measurements delineated in Sec. III.

A. Absorbed power versus electron temperature

As mentioned earlier, the microwave power $P_{\text{ab}} = P_{\text{in}} - P_{\text{out}}$ absorbed by the 2DEG lying underneath the slots of the CPW raises the local electron temperature T_e above the lattice temperature T_L (two-bath model). The heated 2DEG, in turn, transfers the power $P_{\text{e-ph}}$ to the phonons via electron-phonon scattering or P_{diff} to the Ohmic contacts through diffusion. We assume in the present paper that both the lattice temperature T_L and the temperature of the Ohmic contacts are the same as the temperature $T_{\text{bath}} = 50$ mK of the ^3He - ^4He mixture in which the sample is immersed. The power thus flowing out of the 2DEG increases with T_e , and T_e settles to the value at which

$$P_{\text{e-ph}}(T_e, T_L) + P_{\text{diff}}(T_e, T_L) = P_{\text{ab}} \quad (5)$$

holds for a given P_{ab} . The relation Eq. (5) has been used to scrutinize the details of the electron-phonon interaction embodied in the term $P_{\text{e-ph}}(T_e, T_L)$,^{25,26} by examining the relation between the known amount of P_{ab} (introduced to the sample by the Joule heating) and the T_e measured with various methods of thermometry, including the self resistance,^{27–31} the amplitude of the SdHO,^{32–34} thermopower of the ballistic constriction,^{35,36} and the slope of the Hall resistance between two adjacent quantum Hall states.³⁴

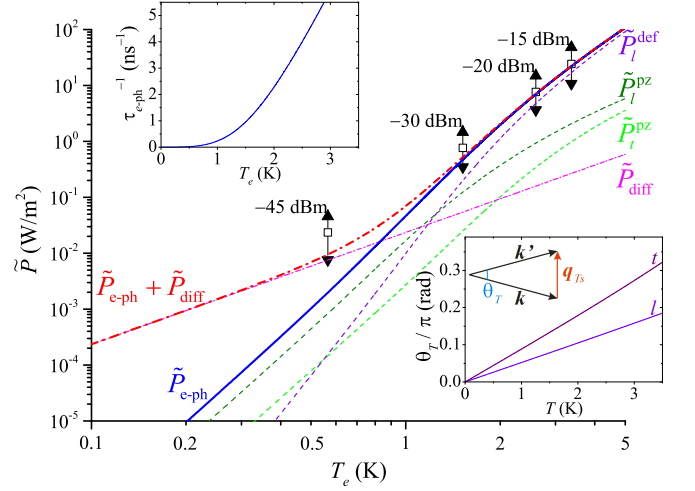


FIG. 5. (Color online) Power absorbed by 2DEG per area \tilde{P}_{ab} vs electron temperature T_e estimated from the SdHO amplitude, plotted in the log-log scale. The square, upward and downward triangles represent the average, the maximum, and the minimum power, respectively, absorbed in the magnetic field range $0.25 \text{ T} < B < 0.6 \text{ T}$. Lines represent calculated energy loss rates per area due to electron-phonon scattering vs T_e , assuming the lattice temperature T_L to be equal to $T_{\text{bath}} = 50$ mK: power loss by deformation potential coupling (\tilde{P}_l^{def}), longitudinal and transverse piezoelectric potential coupling (\tilde{P}_l^{pz} and \tilde{P}_t^{pz}) are plotted by thin dashed lines and their sum ($\tilde{P}_{\text{e-ph}}$, Eq. (7)) by a thick solid line. Roughly estimated energy loss rate by diffusion of electrons into the Ohmic contacts (\tilde{P}_{diff}), and the sum $\tilde{P}_{\text{e-ph}} + \tilde{P}_{\text{diff}}$ are also plotted by thin and thick dot-dashed lines, respectively. Upper inset: Electron-phonon scattering rate calculated by Eq. (18). Lower inset: Scattering angle of the electron-phonon scattering by a typical phonon wavenumber q_{Ts} ($s = l, t$) at the temperature T for longitudinal (l) and transverse (t) phonons.

Following these studies, we plot in Fig. 5 the power per area $\tilde{P}_{\text{ab}} = P_{\text{ab}}/(2wl)$ absorbed from the microwave versus T_e for sample S_{||} taken from the set of the data shown in Fig. 4. Here and in what follows, we use the tilde \tilde{P} and the hat \hat{P} to designate the power per area and the power per electron, respectively, related by $\tilde{P} = \hat{P} \cdot n_e$. The electron temperature T_e is deduced by fitting the amplitude of SdHO at the flat band conditions (where the effect of $V(x)$ on the amplitude vanishes) to the standard formula (an approximation valid for $\mu B \gg 1$),^{37–39}

$$\Delta\sigma_{\text{SdHOamp}} \simeq \frac{\sigma_0}{1 + (\mu B)^2} \exp\left(-\frac{\pi}{\mu_Q B}\right) A\left(2\pi^2 \frac{k_B T_e}{\hbar \omega_c}\right), \quad (6)$$

with $A(X) = X/\sinh(X)$, $\sigma_0 = n_e e \mu$ the conductivity at $B = 0$, μ_Q the quantum mobility,⁴⁰ and $\omega_c = eB/m^*$ the cyclotron angular frequency with m^* the effective mass. The results of the fitting are shown in Fig. 4(b) by dashed lines. The power absorbed by the 2DEG, $P_{\text{ab}} = P_{\text{in}}(1 - \mathcal{P})$, is calculated from \mathcal{P} obtained by the measured $\mathcal{T}(B)$ and Eq. (4), and P_{in} translated from P_{NA} by $P_{\text{in}} =$

$P_{\text{NA}} \cdot 10^{(\mathcal{T}_0/20)}$ with $\mathcal{T}_0 \equiv \mathcal{T}(\sigma_{\alpha\alpha} = 0)$ the transmission (in dB) through the entire circuit in the absence of the attenuation due to the 2DEG.⁴¹ The transmission $\mathcal{T}(B)$ hence P_{ab} varies with B resulting from the variation in $\sigma_{\alpha\alpha}$, and the maximum and minimum values of \tilde{P}_{ab} in the range $0.25 \text{ T} < B < 0.6 \text{ T}$ are indicated in the plots.

In Fig. 5, the plots are compared with calculated curves of $\tilde{P}_{\text{e-ph}}(T_e, T_L)$ and $\tilde{P}_{\text{diff}}(T_e, T_L)$. For the electron-phonon scattering, we basically follow a theory by Price²⁵ (with the correction of a factor of 2 error pointed out in Ref. 30). The formulas used in the calculation are outlined in the subsequent subsection Sec. IV B with the details and subtleties of the approximations employed.

B. Calculation of power loss by electron-phonon scattering as a function of electron temperature

The total electron-phonon energy transfer rate (per area),

$$\tilde{P}_{\text{e-ph}} = \tilde{P}_l^{\text{def}} + \tilde{P}_l^{\text{pz}} + 2\tilde{P}_t^{\text{pz}}, \quad (7)$$

is composed of deformation-potential coupling and piezoelectric coupling contributions (denoted by the superscript $r = \text{def}$ and pz , respectively) with the longitudinal mode (the subscript $s = l$) and two branches of the transverse modes ($s = t$) for the latter coupling. In the strong screening condition (to be discussed below), the constituent components in the $P_{\text{e-ph}}$ can be written down (per electron) as²⁵

$$\hat{P}_s^r(T_e, T_L) = \hat{\Pi}_s^r(T_e) - \hat{\Pi}_s^r(T_L), \quad (8)$$

with

$$\hat{\Pi}_l^{\text{def}}(T) = \frac{1}{\varepsilon_F k_F} \frac{D^2 m^* v_l a_B^{*2}}{16\pi\rho} \left(\frac{k_B T}{\hbar v_l} \right)^7 G_l^{\text{def}}(\kappa_F), \quad (9)$$

and

$$\hat{\Pi}_s^{\text{pz}}(T) = \frac{1}{\varepsilon_F k_F} \frac{(eh_{14})^2 m^* v_s a_B^{*2}}{16\pi\rho} \left(\frac{k_B T}{\hbar v_s} \right)^5 G_s^{\text{pz}}(\kappa_F), \quad (10)$$

where ε_F and k_F represent the Fermi energy and wavenumber, respectively. We used in the calculation the following well-known material parameters for GaAs^{18,42,43}: the deformation potential $D = -9.3 \text{ eV}$, the piezoelectric constant $h_{14} = 1.2 \times 10^9 \text{ V m}^{-1}$, the mass density $\rho = 5.3 \text{ g cm}^{-3}$, the effective Bohr radius $a_B^* = 10.4 \text{ nm}$, the effective mass $m^* = 0.067m_e$ (with m_e the bare electron mass), and the longitudinal and transverse sound velocities $v_l = 5.14 \times 10^3 \text{ m s}^{-1}$ and $v_t = 3.04 \times 10^3 \text{ m s}^{-1}$, respectively. The dimensionless function $G_s^r(\kappa_F)$ is written as²⁵

$$G_s^r(\kappa_F) \equiv \frac{1}{\pi} \int_{-\infty}^{\infty} d\zeta |F(q_{Ts}\zeta)|^2 \times \int_0^{\kappa_F} \frac{d\xi}{\sqrt{1 - (\xi/\kappa_F)^2}} \frac{g_s^r(\xi, \zeta)}{e^{\sqrt{\xi^2 + \zeta^2}} - 1} \frac{1}{H^2(q_{Ts}\xi)} \quad (11)$$

using the form factor,

$$F(q_z) = \int dz |\Phi(z)|^2 e^{iq_z z}, \quad (12)$$

and a function related to the screening,

$$H(q_{\parallel}) = \iint dz_1 dz_2 |\Phi(z_1)|^2 |\Phi(z_2)|^2 e^{-q_{\parallel} |z_1 - z_2|}, \quad (13)$$

which are the functions of the components of the phonon wavevector perpendicular q_z and parallel q_{\parallel} to the 2DEG plane, respectively, and $\Phi(z)$ represents the envelope of the 2DEG wavefunction in the z direction. In Eq. (11), we used $q_{Ts} \equiv k_B T / \hbar v_s$ to normalize $2k_F$ and the components of the phonon wavevector: $\kappa_F \equiv 2k_F / q_{Ts}$, $\xi \equiv q_{\parallel} / q_{Ts}$, and $\zeta \equiv q_z / q_{Ts}$. The kernel $g_s^r(\xi, \zeta)$ in the integral Eq. (11) is given by²⁵

$$g_l^{\text{def}}(\xi, \zeta) \equiv \xi^2 (\xi^2 + \zeta^2)^{3/2}, \quad (14)$$

$$g_l^{\text{pz}}(\xi, \zeta) \equiv \frac{9\xi^6 \zeta^2}{2(\xi^2 + \zeta^2)^{5/2}}, \quad (15)$$

and

$$g_t^{\text{pz}}(\xi, \zeta) \equiv \frac{8\xi^4 \zeta^4 + \xi^8}{4(\xi^2 + \zeta^2)^{5/2}}. \quad (16)$$

In an ideal 2DEG $\Phi(z) = \delta(z)$, we have $|F(q_z)| = H(q_{\parallel}) = 1$. Since q_{Ts} is smaller than the inverse of the rms thickness $\sim 5 \text{ nm}$ of our 2DEG⁴⁴ in the temperature range $T_L < T_e \lesssim 5 \text{ K}$ encompassed in the present study, we can replace $|F(q_z)|$ and $H(q_{\parallel})$ in Eq. (11) by unity to a good approximation. Note that smaller values of ξ and ζ weigh more in Eq. (11) owing to the exponential factor in the denominator $[\exp(\sqrt{\xi^2 + \zeta^2}) - 1]^{-1}$, which derives from the Bose-Einstein distribution of the phonons, $N_s(q, T) = [\exp(q/q_{Ts}) - 1]^{-1}$. The smallness of q_{Ts} also leads to a small value of $a_B^* q_{\parallel}$, allowing the static dielectric function $\epsilon(q_{\parallel}) = 1 + 2H(q_{\parallel})/(a_B^* q_{\parallel})$ to be approximated by $\epsilon(q_{\parallel}) \simeq 2H(q_{\parallel})/(a_B^* q_{\parallel})$. This is the strong screening condition used in the derivation of Eqs. (9) and (10). Using these approximations, we numerically evaluate Eq. (8) and translate the values of $\hat{P}_s^r(T_e, T_L)$ ($r = \text{def}, \text{pz}, s = l, t$) to the power losses per area by

$$\tilde{P}_s^r(T_e, T_L) = \hat{P}_s^r(T_e, T_L) \cdot n_e \quad (17)$$

and plot them along with their sum Eq. (7) in Fig. 5 against T_e . From the energy loss rate, we can also calculate the electron-phonon scattering rate by³⁰

$$\frac{1}{\tau_{\text{e-ph}}} = \frac{1}{C_e} \frac{\partial \tilde{P}_{\text{e-ph}}}{\partial T_e}, \quad (18)$$

where $C_e = (\pi^2 k_B^2 / 3) D(\varepsilon_F) T_e = e^2 L_0 D(\varepsilon_F) T_e$ represents the electron specific heat (per area), with $D(\varepsilon)$ the density of states and $L_0 = \pi^2 k_B^2 / (3e^2) = 2.44 \times 10^{-8} \text{ W}\Omega\text{K}^{-2}$ the Lorenz number. The scattering rate $\tau_{\text{e-ph}}^{-1}$ thus calculated is plotted in the left inset to Fig. 5.

C. Dominant power-loss mechanism and orientational selectivity in the conductivity measurement

We can see in Fig. 5 that, in the measurements carried out with higher microwave powers $P_{\text{NA}} = -30, -20$, and -15 dBm, the predominant power-loss mechanism responsible for determining T_e is the electron-phonon scattering. By contrast, the electron-phonon scattering plays only minor role for the lowest power $P_{\text{NA}} = -45$ dBm. In this case, the energy is transferred mainly through the diffusion of the electrons into the Ohmic contact. We roughly estimate the energy loss rate due to the diffusion using the formula³⁰

$$P_{\text{diff}} = \frac{W}{L} \frac{L_0 \sigma_{xx}}{2} (T_e^2 - T_L^2), \quad (19)$$

with W and L representing the (effective) width and length, respectively, of the path connecting the heated area to the Ohmic contact pads. In Eq. (19), the Wiedemann-Franz law $\kappa_{xx} = L_0 \sigma_{xx} T$ is employed to deduce the thermal conductivity κ_{xx} from the electric conductivity σ_{xx} . The calculated $\tilde{P}_{\text{diff}} = P_{\text{diff}}/(2wl)$ shown in Fig. 5 at least qualitatively explains the deviation at $P_{\text{NA}} = -45$ dBm from the trend $\tilde{P}_{\text{ab}}(T_e) \simeq \tilde{P}_{\text{e-ph}}(T_e)$ followed by the higher power measurements;⁴⁵ it is obvious that $P_{\text{diff}} \propto T_e^2$, having the lowest power 2 for the temperature dependence, becomes the dominant contribution at low enough temperatures.

Figure 5 combined with Fig. 4(c) reveals that when the microwave power injected into the 2DEG from the CPW is dissipated mainly via electron-phonon scattering, the measured conductivity loses the information of the direction of E_{rf} . The intended orientationally-selective measurement is possible only for a weaker microwave power, where the electron-phonon scattering accounts for only a minor portion of the power dissipation. It is natural to relate the loss of the directional selectivity to the large scattering angle the electrons undergo in the electron-phonon scattering events. Scattering angle due to the typical phonon wavenumber q_{Ts} at the temperature T (with $s = l, t$), $\theta_T = 2 \arcsin(q_{Ts}/2k_F)$, is plotted in the right inset of Fig. 5. It shows that, for high P_{NA} with high T_e , the scattering angle due to the electron-phonon scattering⁴⁶ can become much larger than the average scattering angle due to the impurity scattering, $\theta_{\text{imp}} \sim \arccos(1 - \mu_Q/\mu) \sim 0.1\pi$ rad. Note that θ_{imp} is small in modulation doped GaAs/AlGaAs 2DEGs, in which remote ionized donors constitute the major source of the impurity scattering.⁴⁷

It is interesting to point out that, even when the electron-phonon scattering is the main power-loss mechanism, the scattering rate $\tau_{\text{e-ph}}^{-1}$ is still orders of mag-

nitude smaller than the cyclotron frequency ($100 \text{ ns}^{-1} < \omega_c/(2\pi) < 250 \text{ ns}^{-1}$ in $0.25 \text{ T} < B < 0.6 \text{ T}$) or the impurity scattering rate, $\tau_Q^{-1} = e/(m^* \mu_Q) \simeq 430 \text{ ns}^{-1}$; electrons experience numbers of cyclotron revolutions and impurity scatterings, without being disturbed by large-angle scatterings, before passing on the energy gained from the CPW to the phonons. Nevertheless, the direction of E_{rf} is not reflected in the measured conductivity when the electron-phonon scattering is the major route of the power loss. This implies that the whole process, from the initial acceleration of the electrons by E_{rf} to the dumping of the energy thus obtained, should be devoid of large angle scatterings in order for the attenuation of the microwave through the 2DEG to be sensitive only to the component of the conductivity parallel to E_{rf} .

V. CONCLUSIONS

By measuring the attenuation of microwave through a coplanar waveguide (CPW), we have observed commensurability oscillations (CO) in the rf magnetoconductivity of unidirectional lateral superlattices (ULSLs) embedded in the slots of the CPW. Using the phase of the CO as an indicator, we can examine whether or not the component of the conductivity parallel to the rf electric field E_{rf} can be probed selectively. For low microwave power, we find that the component parallel to E_{rf} is detected as expected. With the increase of the microwave power, however, the CO becomes dominated, regardless of direction the principal axis (x axis) of the modulation, by the diffusion contribution which is contained only in σ_{yy} . In the latter power range, the microwave power absorbed by the 2DEG raises the electron temperature T_e so high ($T_e \gtrsim 1.5 \text{ K}$) above the lattice temperature $T_L = 50 \text{ mK}$ that the power is dissipated mainly through the electron-phonon scattering. We attribute the mixing of the component deflected from the direction of E_{rf} to the large scattering angle brought in by the electron-phonon scattering. In order to preserve the intended orientation in the conductivity measurement, the microwave power should be kept low enough to prevent the electron-phonon scattering from becoming the major power loss channel.

ACKNOWLEDGMENTS

This work was supported in part by Grant-in-Aid for Scientific Research (A) (18204029), (B) (20340101), and (C) (22560004) from the Ministry of Education, Culture, Sports, Science and Technology (MEXT).

* akrendo@issp.u-tokyo.ac.jp

¹ L. W. Engel, D. Shahar, Ç. Kurdak, and D. C. Tsui, Phys. Rev. Lett. **71**, 2638 (1993).

- ² P. D. Ye, L. W. Engel, D. C. Tsui, R. M. Lewis, L. N. Pfeiffer, and K. West, *Phys. Rev. Lett.* **89**, 176802 (2002).
- ³ Y. P. Chen, R. M. Lewis, L. W. Engel, D. C. Tsui, P. D. Ye, Z. H. Wang, L. N. Pfeiffer, and K. W. West, *Phys. Rev. Lett.* **93**, 206805 (2004).
- ⁴ Y. P. Chen, G. Sambandamurthy, Z. H. Wang, R. M. Lewis, L. W. Engel, D. C. Tsui, P. D. Ye, L. N. Pfeiffer, and K. W. West, *Nature Phys.* **2**, 452 (2006).
- ⁵ Y. P. Chen, R. M. Lewis, L. W. Engel, D. C. Tsui, P. D. Ye, L. N. Pfeiffer, and K. W. West, *Phys. Rev. Lett.* **91**, 016801 (2003).
- ⁶ R. M. Lewis, Y. Chen, L. W. Engel, D. C. Tsui, P. D. Ye, L. N. Pfeiffer, and K. W. West, *Physica E* **22**, 104 (2004).
- ⁷ H. Zhu, Y. P. Chen, P. Jiang, L. W. Engel, D. C. Tsui, L. N. Pfeiffer, and K. W. West, *Phys. Rev. Lett.* **105**, 126803 (2010).
- ⁸ H. Zhu, G. Sambandamurthy, Y. P. Chen, P. Jiang, L. W. Engel, D. C. Tsui, L. N. Pfeiffer, and K. W. West, *Phys. Rev. Lett.* **104**, 226801 (2010).
- ⁹ R. M. Lewis, P. D. Ye, L. W. Engel, D. C. Tsui, L. N. Pfeiffer, and K. W. West, *Phys. Rev. Lett.* **89**, 136804 (2002).
- ¹⁰ R. M. Lewis, Y. P. Chen, L. W. Engel, D. C. Tsui, P. D. Ye, L. N. Pfeiffer, and K. W. West, *Phys. Rev. Lett.* **93**, 176808 (2004).
- ¹¹ R. M. Lewis, Y. P. Chen, L. W. Engel, D. C. Tsui, L. N. Pfeiffer, and K. W. West, *Phys. Rev. B* **71**, 081301 (2005).
- ¹² G. Sambandamurthy, R. M. Lewis, H. Zhu, Y. P. Chen, L. W. Engel, D. C. Tsui, L. N. Pfeiffer, and K. W. West, *Phys. Rev. Lett.* **100**, 256801 (2008).
- ¹³ H. Zhu, G. Sambandamurthy, L. W. Engel, D. C. Tsui, L. N. Pfeiffer, and K. W. West, *Phys. Rev. Lett.* **102**, 136804 (2009).
- ¹⁴ C. P. Wen, *IEEE Trans. Microwave Theory Tech.* **17**, 1087 (1969).
- ¹⁵ D. Weiss, K. v. Klitzing, K. Ploog, and G. Weimann, *Europhys. Lett.* **8**, 179 (1989).
- ¹⁶ F. M. Peeters and P. Vasilopoulos, *Phys. Rev. B* **46**, 4667 (1992).
- ¹⁷ A. Endo, S. Katsumoto, and Y. Iye, *Phys. Rev. B* **62**, 16761 (2000).
- ¹⁸ A. Endo and Y. Iye, *J. Phys. Soc. Jpn.* **74**, 2797 (2005).
- ¹⁹ A. Endo and Y. Iye, *J. Phys. Soc. Jpn.* **77**, 054709 (2008).
- ²⁰ E. Skuras, A. R. Long, I. A. Larkin, J. H. Davies, and M. C. Holland, *Appl. Phys. Lett.* **70**, 871 (1997).
- ²¹ S. Y. Liao, *Microwave Devices and Circuits* (Prentice Hall, New Jersey, 1990).
- ²² Y. P. Chen, *Quantum Solids of Two Dimensional Electrons in Magnetic Fields*, Ph.D. thesis, Princeton Univ. (2005).
- ²³ We used a carefully chosen function that monotonically decreases with B without any inflection points. This turned out to work better than using the conductivity translated from the high power trace ($P_{\text{NA}} = 0$ dBm) in Fig. 2(a) as a background. Note the remnant non-oscillatory component in Fig. 2(c).
- ²⁴ The amplitude modulation of the SdHO is also wiped out with the increase of P_{NA} , as seen in Fig. 4(b). Although this is mainly due to the dwindling of the SdHO itself with increasing T_e , it can also be affected by the intervention of the counteracting diffusion contribution.
- ²⁵ P. J. Price, *J. Appl. Phys.* **53**, 6863 (1982).
- ²⁶ V. Karpus, *Sov. Phys. Semicond.* **20**, 6 (1986); **21**, 1180 (1987); **22**, 268 (1988).
- ²⁷ A. K. M. Wennberg, S. N. Ytterboe, C. M. Gould, H. M. Bozler, J. Klem, and H. Morkoç, *Phys. Rev. B* **34**, 4409 (1986).
- ²⁸ A. Mittal, M. W. Keller, R. G. Wheeler, D. E. Prober, and R. N. Sacks, *Physica B* **194**, 167 (1994).
- ²⁹ A. Mittal, R. G. Wheeler, M. W. Keller, D. E. Prober, and R. N. Sacks, *Surf. Sci.* **361**, 537 (1996).
- ³⁰ A. Mittal, in *Quantum Transport in Semiconductor Submicron Structures*, edited by B. Kramer (Kluwer Academic, Dordrecht, 1996) p. 303.
- ³¹ E. Chow, H. P. Wei, S. M. Girvin, W. Jan, and J. E. Cunningham, *Phys. Rev. B* **56**, R1676 (1997).
- ³² K. Hirakawa and H. Sakaki, *Appl. Phys. Lett.* **49**, 889 (1986).
- ³³ Y. Ma, R. Fletcher, E. Zaremba, M. D'Iorio, C. T. Foxon, and J. J. Harris, *Phys. Rev. B* **43**, 9033 (1991).
- ³⁴ E. Chow, H. P. Wei, S. M. Girvin, and M. Shayegan, *Phys. Rev. Lett.* **77**, 1143 (1996).
- ³⁵ N. J. Appleyard, J. T. Nicholls, M. Y. Simmons, W. R. Tribe, and M. Pepper, *Phys. Rev. Lett.* **81**, 3491 (1998).
- ³⁶ C. R. Proetto, *Phys. Rev. B* **44**, 9096 (1991).
- ³⁷ T. Ando, A. B. Fowler, and F. Stern, *Rev. Mod. Phys.* **54**, 437 (1982).
- ³⁸ A. Isihara and L. Smrčka, *J. Phys. C: Solid State Phys.* **19**, 6777 (1986).
- ³⁹ A. Endo, N. Hatano, H. Nakamura, and R. Shirasaki, *J. Phys.: Condens. Matter* **21**, 345803 (2009).
- ⁴⁰ We used $\mu_Q = 6.15 \text{ m}^2\text{V}^{-1}\text{s}^{-1}$ deduced from the SdHO in the magnetoresistivity measured separately with a Hall bar device fabricated from the same 2DEG wafer as that used for samples S_{\perp} and S_{\parallel} .
- ⁴¹ Here, we used the fact that the incoming and outgoing coaxial cable circuitry is symmetric.
- ⁴² S. Adachi, *J. Appl. Phys.* **58**, R1 (1985).
- ⁴³ S. K. Lyo, *Phys. Rev. B* **38**, 6345 (1988); *Phys. Rev. B* **40**, 6458 (1989).
- ⁴⁴ A. Endo and Y. Iye, *J. Phys. Soc. Jpn.* **74**, 1792 (2005).
- ⁴⁵ To apply the formula Eq. (19) intended for a rectangular sample to our complicatedly shaped sample (see the inset of Fig. 1(c)), we resorted to drastic approximation: we used the values of W/L taken from the thinnest part of the legs leading to the six Ohmic contact pads, and the value of σ_{xx} at $B = 0$, hoping that the cancellation of the under- and overestimating nature of the two treatments yields the right order of magnitude. The ambiguity in the quantitative estimate of P_{diff} does not affect the main conclusion of the present paper.
- ⁴⁶ The scattering angle is primarily determined by the phonons at the temperature T_e , not the lattice temperature T_L . Note the dominance of the first term in Eq. (8), which contains the Bose-Einstein distribution with the temperature T_e , $N_s(q, T_e)$ (see Eqs. (8)–(11)).
- ⁴⁷ J. H. Davies, *The physics of low-dimensional semiconductors* (Cambridge University Press, 1998).